Control of Flapwise Vibrations in Wind Turbine Blades using semi-active tuned mass dampers

By

John Arrigan[1], Vikram Pakrashi[2], Biswajit Basu[3] and Satish Nagarajaiah[4]*

[1,2,3]Department of Civil, Structural and Environmental Engineering, Trinity College Dublin, Ireland

[4] Department of Civil and Env. Eng. and Mech. Eng. and Mat. Sc., Rice University, Houston, TX, United States

E-mail: [1]arriganj@tcd.ie, [2] pakrashv@tcd.ie, [3]basub@tcd.ie, [4]nagaraja@rice.edu

** Corresponding Author*

Abstract

The increased size and flexibility of modern multi-Megawatt wind turbines has resulted in the dynamic behaviour of these structures becoming an important design consideration. The aim of this paper is to study the variation in natural frequency of wind turbine blades due to centrifugal stiffening, and the potential use of Semi-Active Tuned Mass Dampers (STMDs) in reducing vibrations in the flapwise direction with changing parameters in the turbine. The parameters considered were the rotational speed of the blades and the stiffness of the blades and nacelle. Two techniques have been employed to determine the natural frequency of a rotating blade. The first employs the Frobenius method to a rotating Bernoulli-Euler beam. These results are compared to the natural frequencies determined from an eigenvalue analysis of the dynamic model of the turbine including nacelle motion which is developed in this paper. The model derived considers the structural dynamics of the turbine and includes the dynamic coupling

between the blades and tower. The semi-active control system developed employs a frequency tracking algorithm based on the Short Time Fourier Transform (STFT) technique. This is used to continually tune the dampers to the dominant frequencies of the system. Numerical simulations have been carried out to study the effectiveness of the STMDs in reducing flapwise vibrations in the system when variations occur in certain parameters of the turbine. Steady and turbulent wind loading has been considered.

1 INTRODUCTION

Wind turbines with outputs as large as 5MW are being constructed with tower heights and rotor diameters of over 80m and 120m respectively. As a result of the increasing size of the turbine components, the blades are becoming the limiting factor towards larger even more powerful turbines. Significant research has already been carried out into the dynamic behaviour of wind turbines. Rauh and Peinke (1) developed a model to study their dynamic response. Tavner et al. (2) performed a study into the reliability of large wind turbines. They noted that the installation of turbines in more remote locations, particularly offshore gives rise to the need for more accurate reliability analysis so that wind turbine availability and design life can be predicted.

With the increased size of the turbine blades comes increased flexibility making it important to understand their dynamic behaviour. Sutherland (3) studied the fatigue properties of the different materials used in wind turbines from the steel in the tower to the composites used in blade design. Ahlstrom carried out research into the effect of increased flexibility in turbine blades and found that it can lead to a significant drop in the power output of the turbine (4). Significant research has been carried out into the area of blade design and their failure characteristics (5, 6, 7). However, it is only over the last few years that research has started to focus on the dynamic

behaviour of the turbine blades and the dynamic interaction that occurs between the blades and the tower.

Two main types of vibration occur in wind turbine blades, flapwise and edgewise. Flapwise vibrations are vibrations occurring out of the plane of rotation of the blades while edgewise vibrations occur in the plane of rotation. Flapwise vibration is similar in nature to the phenomenon of fluttering in aircraft wings and in extreme cases has lead to the turbine blades colliding with the tower resulting in catastrophic failure of the structure. Ronold and Larsen (8) studied the failure of a wind turbine blade in flapwise bending during normal operating conditions of the turbine. Murtagh and Basu (9) studied the flapwise motion of wind turbine blades and included their dynamic interaction with the tower. They found that inclusion of the blade-tower interaction could lead to significant increases in the maximum blade tip displacement.

Efforts to mitigate the increased vibration problems that are occurring in wind turbine blades have thus far concentrated on the actual design of the blades themselves. This has focussed on attempting to increase the structural damping present in them or alter their aerodynamic properties (10, 11). The possibility of using dampers in the blades to control their dynamic behaviour has not yet been investigated in detail.

Vibration mitigating devices have been used in engineering systems for many decades; Tuned Mass Dampers (TMDs) being one of the first types. TMDs consist of a mass connected to the primary structure through the use of springs and dashpots. Passive TMDs have been used widely throughout civil engineering applications, particularly in tall buildings subjected to wind or earthquake loadings. One of the first buildings to have a TMD installed was the John Hancock Building in Boston. Extensive research has been carried out into the use of passive TMDs and

their suitability for vibration control (12, 13, 14, 15). The non-linearity of nearly all engineering dynamical systems has raised the need for Semi-Active TMDs (STMDs) due to their ability to adjust their tuning to cater for changes in the behaviour of the primary system. Semi-active devices are more desirable than active as they require significantly less power and are therefore more cost effective. Pinkaew and Fujino (16) looked at the use of STMDs for vibration mitigation in structures excited by harmonic loads. Nagarajaiah and Varadarajan (17), and Nagarajaiah and Sonmez (18) applied Short Time Fourier Transform (STFT) techniques to track the dominant frequencies of the system being damped. This allowed the STMD to be continually tuned to the dominant frequency of the structure resulting in a more effective reduction in response.

The aim of this paper is to investigate the effectiveness of STMDs in the vibration control of wind turbine blades. Investigation into the natural frequencies of rotating blades is also considered for different rotational speeds. Two techniques have been employed for comparison. The first considers the natural frequencies of a rotating Bernoulli-Euler cantilever beam using the Frobenius method. This is then compared to the frequencies obtained from an eigenvalue analysis of the turbine model developed in this paper.

The hollow nature of wind turbine blades makes them naturally suitable for the use of internal damping devices. However, thus far, little work has been done investigating this possibility. Most of the current research into the dynamic behaviour of wind turbine blades has focused on aerodynamic models of the blades themselves. The model developed in this paper looks purely at the structural dynamics of the turbine including the blade-tower interaction. Flapwise vibration only has been considered.

The model presented consists of three rotating cantilever beams (representing the turbine blades) connected at their root to a large mass (which models the nacelle) allowing the inclusion of blade-tower interaction. The masses, lengths, natural frequencies etc. were chosen to replicate those of a real wind turbine to accurately capture the dynamic interaction between the blades and nacelle. An STMD was connected to each blade tip and to the nacelle. This gave the completed model including STMDs a total of 8 Degrees of Freedom (DOF). Steady and turbulent wind loading was applied to the model acting in the flapwise direction.

2 ANALYSIS FOR CALCULATION OF NATURAL FREQUENCIES

2.1 Determination of Blade Natural Frequencies Using Frobenius Method

The governing differential equation for a rotating Euler Bernoulli beam with rigid support under flapwise vibration is

$$\rho A \frac{\partial^2 w}{\partial t^2} + \frac{\partial^2}{\partial x^2}\left(EI \frac{\partial^2 W}{\partial t^2} \right) - \frac{\partial}{\partial x}\left(T \frac{\partial w}{\partial x} \right) = f(x,t) \tag{1}$$

where ρ is the density of the beam, A is the cross sectional area, w is the relative displacement of a point with respect to its static deflected position, E is the Young's modulus of elasticity of the material of the beam, I is the moment of inertia of the beam about its relevant axis, T is the centrifugal tension force on the beam at a point x with respect to the origin and f is the applied force per unit length on the beam. The cross sectional area, A, and bending rigidity, EI, are taken as constant along the length of the beam, x. Both w and f are dependent on the location on the beam with respect to the origin, x, and time, t. The centrifugal tension T is expressed as

$$T(x) = \int_{x}^{L} \rho A \Omega^2 (r + x) dx \tag{2}$$

where L is the length of the beam, r is the radius of the rigid hub to which the flexible beam is attached and Ω is the angular velocity of rotation of the beam, which is assumed to be constant. The effect of gravity on the rotation of the beam is assumed negligible compared to the centrifugal effect.

The non-dimensional rotational speed parameter and natural frequency parameters are defined as

$$\nu = \eta^2 = \frac{\rho A \Omega^2 L^4}{EI} \tag{3}$$

and

$$\mu = \overline{\Omega}^2 = \frac{\rho A \omega^2 L^4}{EI} \tag{4}$$

respectively where ω is the natural frequency of the beam. Setting *f(x,t)* = 0 in equation 1 and substituting the non-dimensional parameters, the modeshape equation is obtained in a dimensionless form as

$$D^4 W(X) - 0.5\nu(1 + 2\rho_0) D^2 W(X) + \nu \rho_0 D[XDW(X)] + 0.5\upsilon D\left(X^2 DW(X) - \mu W(X)\right) = 0 \tag{5}$$

where $$D = \frac{d}{dX},\ X = \frac{x}{L},\ W(X,t) = \frac{w(x,t)}{L} \text{ and } \rho_0 = \frac{r}{L} \tag{6}$$

Employing the Frobenius method of series solution of differential equations as in (19) and considering ideal clamped-free boundary conditions for a cantilever, the natural frequency equation is obtained to be

$$D^2F(1,2)D^3F(1,3) - D^3F(1,2)D^2F(1,3) = 0 \tag{7}$$

where

$$F(X,c) = \sum a_{n+1}(c)X^{c+n} \tag{8}$$

By choosing

$$a_1(c) = 1,\ a_2(c) = 0,\ a_3(c) = \frac{0.5\nu(1+2\rho_0)}{(c+2)(c+1)} \text{ and } a_4(c) = \frac{-\nu\rho_0 c}{(c+3)(c+2)(c+1)} \tag{9}$$

the recurrence relation is obtained as

$$\begin{aligned}&(c+n+4)(c+n+3)(c+n+2)(c+n+1)a_{n+5}(c) - 0.5\nu(1+2\rho_0)(c+n+2)(c+n+1)a_{n+3}(c)\\&+\nu\rho_0(c+n+1)^2 a_{n+2}(c) + [0.5\nu(c+n)(c+n+1) - \mu]a_{n+1}(c) = 0\end{aligned} \tag{10}$$

The normalised modeshape equation can be derived as

$$\Phi_n(X) = \frac{\left[D^2F(1,3)F(X,2) - D^2F(1,2)F(X,3)\right]}{\left[D^2F(1,3)F(1,2) - D^2F(1,2)F(1,3)\right]} \tag{11}$$

It is important to note that for an Euler Bernoulli rotating beam with double symmetric cross section, it can be shown that the in plane and out of plane vibrations are uncoupled and the respective natural frequencies differ by a constant equal to the square of the non-dimensional rotational speed. This paper considers only the out of plane or flapwise vibrations. The results obtained using the Frobenius technique are discussed later in the paper. The formulation does not consider the motion of the nacelle at the base of the blade.

3 LAGRANGIAN FORMULATION

3.1 Dynamic Model including Nacelle Motion

The dynamic model was formulated using the Lagrangian formulation expressed in equation 12 below

$$\frac{d}{dt}\left(\frac{\delta T}{\delta \dot{q}_i}\right) - \frac{\delta T}{\delta q_i} + \frac{\delta V}{\delta q_i} = Q_i \tag{12}$$

where: T = kinetic energy of the system, V = potential energy of the system, q_i = displacement of the generalized degree of freedom i and Q_i = generalized loading for degree of freedom i. The kinetic and potential energies of the model were first derived including the motion of the nacelle and are stated in equations 13a and 13b. These expressions were then substituted back into the Lagrangian formulation in equation 12 to allow the equations of motion to be determined.

$$T = \frac{1}{2} m_b \sum_{i=1}^{3} \int_0^L {v_{bi}}^2 dx + \frac{1}{2} M_{nac} {\dot{q}_{nac}}^2 \tag{13a}$$

$$V = \frac{1}{2} EI \sum_{i=1}^{3} \int_{0}^{L} \left(\frac{\delta^2 q_i}{\delta x^2} \right)^2 dx + \frac{1}{2} K_{nac} q_{nac}{}^2 \tag{13b}$$

where: m_b = mass of blade, L = length of the blade (= 48m), v_{bi} = velocity of blade tip 'i' including the nacelle motion that causes blade tip displacement, M_{nac} = mass of nacelle, E = Young's Modulus for the blade, I = second moment of area of blade, K_{nac} = stiffness of the nacelle, q_i is the displacement of the blade i and q_{nac} is the displacement of the nacelle.

Each blade was modelled as a cantilever beam with uniformly distributed parameters as can be observed from the expressions for the kinetic and potential energies in equations 13a and 13b. They were assumed to be vibrating in their first mode with a quadratic modeshape. The cantilevers were attached at their root to a large mass representing the nacelle of the turbine. This allowed for the inclusion of the blade-tower interaction in the model. STMDs were attached to the system, modelled as mass-spring-dashpot systems whose tuning was controlled by the semi-active algorithm outlined later in this paper. A schematic of the model is shown in figure 1. The degrees of freedom (dof) marked q_1, q_2, q_3 and q_{nac} represent the motion of the blades and nacelle and the STMD displacements are labelled as d_i, where i corresponds to the relevant dof. For simplicity just two STMDs are shown in the diagram. One attached to the nacelle and the other attached to the blade in the upright vertical position.

The final model with STMDs attached consisted of a total of 8 dof (with a total of four dampers, one in each of the blades and one at the nacelle) expressed in the standard form as in equation 14 below.

$$[M]\{\ddot{q}\} + [C]\{\dot{q}\} + [K]\{q\} = \{Q\} \tag{14}$$

where [*M*], [*C*] and [*K*] are the mass, damping and stiffness matrices of the system respectively. $\ddot{q}$, $\dot{q}$ and q are the acceleration, velocity and displacement vectors and Q is the loading. Centrifugal stiffening was added to the model as per the formula developed by Hansen (20). Structural damping included in the system was assumed to be in the form of stiffness proportional damping.

3.2 Loading

Two simple load cases were studied in this paper. The first loading scenario looked at the effect of a steady wind load that varied linearly with height. The rotation of the blades meant that the loading on each blade was time dependant as they moved through the wind field. Since a couple of harmonic terms arose in the loading it was simplified to just the first harmonic so the performance of the STMDs could be assessed for this simpler load case. Equation 15 shows the expression for the loading on blade 1. The loads on blades 2 and 3 are shifted by angles of $2\pi/3$ and $4\pi/3$ respectively.

$$Q_1 = \left(\frac{v_{nac}{}^2 A}{3} + \frac{v_{nac+L}{}^2 A}{10} \right) + \left(\frac{v_{nac} v_{nac+L} A}{2} \right) \cos(\Omega t) \tag{15}$$

where: v_{nac} = wind speed at nacelle height, v_{nac+L} = wind speed at the maximum blade tip height, i.e. when blade is in upright vertical position. A = Area of blade, taken as 1 to normalize the load, with Ω as before equal to the rotational speed of the blade. The loading on the nacelle was assumed to be zero so that all motion of the nacelle was due to the forces transferred from the blades through the coupling present in the system.

The second loading scenario considered the same load case as the first but with an added random component modelling turbulent wind. This turbulent velocity component was generated at a height equal to that of the nacelle using a Kaimal spectrum (21) defined by equations 16, 17 and 18 below. Uniform turbulence was assumed for the blades.

$$\frac{fS_{vv}(H, f)}{v_*^2} = \frac{200c}{(1+50c)^{\frac{5}{3}}} \tag{16}$$

where: H = nacelle height, $S_{vv}(H, f)$ is the PSDF (Power Spectral Density Function) of the fluctuating wind velocity as a function of the hub elevation and frequency, v_* is the friction velocity from equation 17, and c is known as the Monin coordinate which comes from equation 18.

$$\bar{v}(H) = \frac{1}{k} v_* \ln \frac{H}{z_0} \tag{17}$$

$$c = \frac{fH}{\bar{v}(H)} \tag{18}$$

where k is Von-Karman's constant (typically around 0.4 (22)), z_0 = 0.005 (the roughness length), and $\bar{v}(H)$ is the mean wind speed. This results in a turbulence intensity of 0.115 in the generated spectrum.

4 STFT BASED TRACKING ALGORITHM

STFT is a commonly used method of identifying the time-frequency distribution of non-stationary signals. It allows local frequencies to be picked up in the response of the system that may only exist for a short period of time. These local frequencies can be missed by normal Fast Fourier Transform (FFT) techniques. The STFT algorithm splits up the signal into shorter time segments and an FFT is performed on each segment to identify the dominant frequencies present in the system during the time period considered. Combining the frequency spectra of each of these short time segments results in the time frequency distribution of the system over the entire time history.

The STFT algorithm developed in this study allows the STMDs to be tuned in real-time to the dominant frequencies in the system. Before each time segment is Fourier analyzed it is multiplied by a window function centred on the time of interest. In this case the time of interest is the current time of the response to allow for real-time tuning. A Hanning window function has been employed in this paper, emphasising the frequencies just before the current time. Once the weighted signal is obtained an FFT is performed and the frequency spectrum obtained. The dominant frequencies are then identified and the STMDs tuned to these frequencies. The algorithm is repeated every second allowing the tuning of the STMDs to be adjusted in real-time as the frequencies present in the system change. The amount the tuning of the STMD could vary from one call of the STFT algorithm to the next was limited to prevent the build up of transience in the system. This could lead to sudden increases in response amplitude. The semi-active algorithm is outlined in the flow chart shown in figure 2.

5 RESULTS

5.1 Natural frequency estimation

The natural frequency was first calculated using the Frobenius method for a stationary Bernoulli Euler beam, i.e. $\Omega = 0$. This value was then used in the Lagrangian dynamic model with the effect of centrifugal stiffening added in, which is dependent on the rotational speed, Ω. Natural frequencies for 3 other rotational speeds were then obtained. The Frobenius method results for the Bernoulli Euler beam were compared to two different cases from Lagrangian analysis. The first was a single rotating uniform cantilever beam assuming the nacelle motion to be zero. The second was a 3 blade turbine model which included blade tower interaction. A 14^{th} term expansion was deemed sufficient for the Frobenius results. All natural frequencies calculated are for the first mode of vibration. Higher modes can be calculated easily using the Frobenius technique. The results for the first mode are shown in Table 1. It can be seen that there is a good agreement between the Frobenius results and the Lagrangian single blade model. For the full 3 blade model including nacelle coupling all three blade natural frequencies are listed. As can be seen two of these are in good agreement with the Frobenius results while the third is significantly different. This is a result of the interaction between the blades and nacelle. Omission of the nacelle coupling results in 3 identical natural frequencies for the blades which are in close agreement with the Lagrangian single blade and Frobenius results.

5.2 Dynamic control – Steady wind load

The following section looks at the results of the STMD system for the steady wind loading described above in section 2.3. The model was run with all parameters constant (Ω, ω_b and ω_{nac}) so the response of the system could be observed under normal operating conditions of the turbine. Figure 3a and 3b shows the frequency content of the blade and the nacelle respectively.

Vary Ω, rotational speed of the blades

The first parameter varied was the rotational speed of the blades, Ω. The variation considered the blades slowing down linearly over 180 seconds from 3.14 rads/s to 1.57 rads/s. The natural frequency of the blades and nacelle were kept constant. Figure 4a shows the undamped and damped response of one of the blades with figure 4b showing the corresponding STMD behaviour by plotting the blade displacement, STMD displacement and STMD tuning all with respect to time. This allows an insight into the behaviour of the semi-active algorithm. As can be seen in figure 4a a significant reduction is achieved in the response of the blade. The behaviour of the STMD in figure 4b clearly shows the semi-active behaviour kicking in at t = 41 seconds and the tuning of the STMD changing with respect to time.

The nacelle response and STMD behaviour is illustrated in figures 5a and 5b. A large reduction is again achieved when the STMD kicks in at t = 41 seconds.

Vary ω_{b1}, the natural frequency of blade 1

The natural frequency of blade 1 was varied from 1.5588 Hz (9.79 rads/s) to 1.2398 Hz (7.79 rads/s) at t = 100 seconds. This loss of blade stiffness simulates damage occurring in the blade. The other two blades were assumed to remain unchanged.

Figure 6a plots the displacement response of blade 1. As can be observed at t = 100 seconds the behaviour of the blade changes due to the change in its natural frequency. The tuning of the STMD adapts for this as can be seen in figure 6b. This results in an effective reduction in the response of the blade before and after the change in natural frequency, as can be observed in figure 6a.

The corresponding nacelle plots are shown in figures 7a and 7b. Again the algorithm identifies the shift in system behaviour and takes this into account, thus achieving a response reduction before and after the change in the natural frequency of blade 1.

Vary ω_{nac}, the natural frequency of the nacelle

The natural frequency of the nacelle was then varied from 0.5675 Hz (3.566 rads/s) to 0.4775 Hz (3 rads/s) at t = 100 seconds, simulating damage to the tower of the turbine.

The displacement response of blade 1 is plotted in figure 8a with the corresponding STMD behaviour shown in figure 8b. No real shift in blade behaviour is seen at t =100 seconds. This suggests that the frequency of the tower doesn't have a large bearing on the blade response. However, this could also be a result of the fact that no load is considered to act on the nacelle. A good reduction is again seen in the blade with the STMD.

The same is seen for the nacelle results in figures 9a and 9b. As expected the semi-active algorithm achieves a good reduction in response. A slight change can be seen in the tuning of the nacelle STMD due to the shift in natural frequency but clearly this shift is not enough to cause a noticeable change in the nacelle's behaviour.

5.3 Dynamic control –Turbulent wind load

Response of the model to the turbulent wind load described in section 2.3 was also investigated. This turbulent loading considered the same steady wind speed at the nacelle but with an added turbulent component modelled by a Kaimal spectrum. The same parametric variations were considered as for the steady wind load.

Vary Ω, the rotational speed of the blades

Figures 10a and 10b plot the displacement response of blade 1 and the corresponding STMD behaviour. The semi-active algorithm again caters well for the turbulent loading achieving a significant reduction in response. The nacelle results are shown in figures 11a and 11b. Again a good reduction is seen in the response of the turbine. The tuning of the nacelle STMD can be seen in figure 11b.

Vary ω_{b1}, the natural frequency of blade 1

Good reduction is again seen in the blade response both before and after the change in natural frequency which occurs at t = 70 seconds. This can be observed in figure 12a. The STMD behaviour can be seen in figure 12b. A large reduction is also achieved in the nacelle displacement before and after the change in the natural frequency of blade 1, as can be seen in figure 13a. The behaviour of the nacelle STMD is plotted in figure 13b.

Vary ω_{nac}, the natural frequency of the nacelle

Finally, the nacelle natural frequency was varied as before, again at t = 70 seconds for the turbulent wind load. Figures 14a and 15a show the STMD achieving a reduction in both the blade and nacelle responses. Similar to the steady wind load results, no real change is seen in the model's behaviour after the change in nacelle natural frequency. This can again be attributed to the fact that a greater change in nacelle natural frequency is needed to alter the behaviour of the system. The tuning of the blade and nacelle STMDs can be seen in figures 14b and 15b respectively.

6 CONCLUSIONS

In this study, the use of STMDs to control wind turbine blades in flapwise bending has been investigated. An STFT based algorithm has been used for semi-active tuning. The model developed in this paper focussed only on the structural dynamics of the turbine including the interaction between the blades and the tower. The natural frequency of the rotating blades for different rotational speeds, Ω, were calculated using a Lagrangian model by performing an eigenvalue analysis on the system. These results were compared to those obtained by applying the Frobenius method to a rotating Bernoulli Euler beam with the same stationary natural frequency. Good agreement was seen between the models and the methods used.

Four STMDs were added to the model, one at each blade tip and one at the nacelle to control the response of each component. The displacement response of the system was controlled in real time by processing a previous window of 40 seconds and feeding back the information into the semi-active algorithm. This 40 second window allowed a frequency of 0.025Hz to be captured which is the incremental frequency for retuning of the STMDs. This ensures no mistuning of the dampers. The windowed time segment was then Fourier analysed to determine the dominant frequencies in the system at the current time. The STMDs were then repeatedly tuned every second in real-time according to this algorithm. A Hanning window function was employed.

Numerical simulations were carried out to ascertain the effectiveness of the STMDs in mitigating flapwise vibrations in the model when variations were considered in three of the system parameters. The parameters varied were the rotational speed, Ω, the natural frequency of blade 1, ω_{b1}, and the natural frequency of the nacelle, ω_{nac}. This allowed the simulations to take account of changes in system parameters during operational conditions of the turbine due to environmental changes, or damage in the blades and nacelle which may occur during the life

cycle of the turbine. Significant reduction was achieved by the semi-active algorithm for both steady and turbulent wind loading highlighting the viability of STMDs in controlling flapwise vibrations in wind turbines. Further studies by the authors into the investigation and control of edgewise vibrations in the blades are currently being undertaken.

References

[1] A. Rauh and J. Peinke, "A phenomenological model for the dynamic response of wind turbines to turbulent wind", *Journal of Wind Engineering and Industrial Aerodynamics*, vol. 92, 2004, pp 159-183.

[2] P. J. Tavner, J. Xiang, and F. Spinato, "Reliability Analysis for Wind Turbines," Wind Energy, 2006.

[3] H. J. Sutherland, "A Summary of the Fatigue Properties of Wind Turbine Materials", *Wind Energy*, vol. 3, 2000, pp 1-34.

[4] A. Ahlstrom, "Influence of Wind Turbine Flexibility on Loads and Power Production", *Wind Energy*, vol. 9, 2005, pp 237-249.

[5] C. Kong, J. Bang, and Y. Sugiyama, "Structural investigation of composite wind turbine blade considering various load cases and fatigue life", *Energy*, vol. 30, 2005, pp 2101-2114.

[6] M. E. Bechly and P. D. Clausen, "Structural Design of a composite wind turbine blade using Finite Element Analysis", *Computers and Structures*, vol. 63, 1997, pp 639-646.

[7] F. M. Jensen, B. G. Falzon, J. Ankersen, and H. Stang, "Structural testing and numerical simulation of 34m composite wind turbine blade", *Composite Structures*, vol. 76, 2006, pp 52-61.

[8] K. O. Ronold and G. C. Larsen, "Reliability-based design of wind-turbine rotor blades against failure in ultimate loading", *Engineering Structures*, vol. 22, 2000, pp 565-574.

[9] P. J. Murtagh, B. Basu, and B. M. Broderick, "Along-wind response of a wind turbine tower with blade coupling subjected to rotationally sampled wind loading", *Engineering Structures*, vol. 27, 2005, pp 1209-1219.

[10] P. K. Chaviaropoutos, E. S. Politis, D. J. Lekou, N. N. Sorensen, M. H. Hansen, B. H. Bulder, D. Winkelaar, C. Lindenburg, D. A. Saravanos, T. P. Philippidis, C. Galiotis, M. O. L. Hansen, and T. Kossivas, "Enhancing the Damping of Wind Turbine Rotor Blades, the DAMPBLADE Project", *Wind Energy*, vol. 9, 2006, pp 163-177.

[11] P. K. Chaviaropoutos, I. G. Nikolaou, K. A. Aggelis, N. N. Sorensen, J. Johansen, M. O. L. Hansen, M. Gaunaa, T. Hambraus, H. F. von Geyr, C. Hirsch, K. Shun, S. G. Voutsinas, G. Tzabiras, J. Perivolaris, and S. Z. Dyrmose, "Viscous and Aeroelastic Effects on Wind Turbine Blades. The VISCEL Project. Part 1: 3D Navier-Stokes Rotor Simulations", *Wind Energy*, vol. 6, 2003, pp 365-385.

[12] J. W. Hijmissen and W. T. Van Horssen, "On aspects of damping for a vertical beam with a tuned mass damper at the top", *Nonlinear Dynamics*, vol. 50, 2007, pp 169-190.

[13] C. C. Chang, "Mass dampers and their optimal designs for building vibration control", *Engineering Structures*, vol. 21, 1999, pp 454-463.

[14] H.-N. Li and X.-L. Ni, "Optimization of non-uniformly distributed multiple tuned mass damper", *Journal of Sound and Vibration*, vol. 308, 2007, pp 80-97.

[15] A. Kareem and S. Kline, "Performance of multiple mass dampers under random loading", *Journal of Structural Engineering*, vol. 121, 1995, pp 348-361.

[16] T. Pinkaew and Y. Fujino, "Effectiveness of semi-active tuned mass dampers under harmonic excitation", *Engineering Structures*, vol. 23, 2001, pp 850-856.

[17] S. Nagarajaiah and N. Varadarajan, "Short time Fourier transform algorithm for wind response control of buildings with variable stiffness TMD", *Engineering Structures*, vol. 27, 2005, pp 431-441.

[18] S. Nagarajaiah and E. Sonmez, "Structures with Semiactive Variable Stiffness Single/Multiple Tuned Mass Dampers," *Journal of Structural Engineering*, vol. 133, 2007, pp 67-77.

[19] S. Naguleswaran, "Lateral Vibration of a Centrifugally Tensioned Uniform Euler-Bernoulli Beam", *Journal of Sound and Vibration*, vol. 176, 1994, pp 613-624.

[20] M. H. Hansen, "Improved Modal Dynamics of Wind Turbines to Avoid Stall-Induced Vibrations", *Wind Energy*, vol. 6, 2003, pp 179-195.

[21] J. C. Kaimal, J. C. Wyngaard, Y. Izumi, and O. R. Coté, "Spectral characteristics of surface-layer turbulence", *Quarterly Journal of the Royal Meteorological Society*, vol. 98, 1972, pp 563-589.

[22] E. Simiu and R. Scanlan, Wind Effects on Structures, 3rd ed., John Wiley & Sons, New York, 1996.

List of Figures

Figure 1 Dynamic model

Figure 2 Semi-active Algorithm

Figure 3a Blade Frequency Response, Ω = 3.14 rads/s, ω_b = 10 rads/s, ω_{nac} = 3.566rads/s

Figure 3b Nacelle Frequency Response, Ω = 3.14 rads/s, ω_b = 10 rads/s, ω_{nac} = 3.566rads/s

Figure 4a Displacement Response of Blade 1, Varying Ω, Steady wind load

Figure 4b Blade 1 STMD Behaviour, Varying Ω, Steady wind load

Figure 5a Displacement Response of Nacelle, Varying Ω, Steady wind load

Figure 5b Nacelle STMD Behaviour, Varying Ω, Steady wind load

Figure 6a Displacement Response of Blade 1, Varying ω_b, Steady wind load

Figure 6b Blade 1 STMD Behaviour, Varying ω_b, Steady wind load

Figure 7a Displacement Response of Nacelle, Varying ω_b, Steady wind load

Figure 7b Nacelle STMD Behaviour, Varying ω_b, Steady wind load

Figure 8a Displacement Response of Blade 1, Varying ω_{nac}, Steady wind load

Figure 8b Blade 1 STMD Behaviour, Varying ω_{nac}, Steady wind load

Figure 9a Displacement Response of Nacelle, Varying ω_{nac}, Steady wind load

Figure 9b Nacelle STMD Behaviour, Varying ω_{nac}, Steady wind load

Figure 10a Displacement Response of Blade 1, Varying Ω, Turbulent loading

Figure 10b Blade 1 STMD Behaviour, Varying Ω, Turbulent loading

Figure 11a Displacement Response of Nacelle, Varying Ω, Turbulent wind load

Figure 11b Nacelle STMD Behaviour, Varying Ω, Turbulent wind load

Figure 12a Displacement Response of Blade 1, Varying ω_b, Turbulent wind load

Figure 12b Blade 1 STMD Behaviour, Varying ω_b, Turbulent wind load

Figure 13a Displacement Response of Nacelle, Varying ω_b, Turbulent wind load

Figure 13b Nacelle STMD Behaviour, Varying ω_b, Turbulent wind load

Figure 14a Displacement Response of Blade 1, Varying ω_{nac}, Turbulent wind load

Figure 14b Blade 1 STMD Behaviour, Varying ω_{nac}, Turbulent wind load

Figure 15a Displacement Response of Nacelle, Varying ω_{nac}, Turbulent wind load

Figure 15b Nacelle STMD Behaviour, Varying ω_{nac}, Turbulent wind load

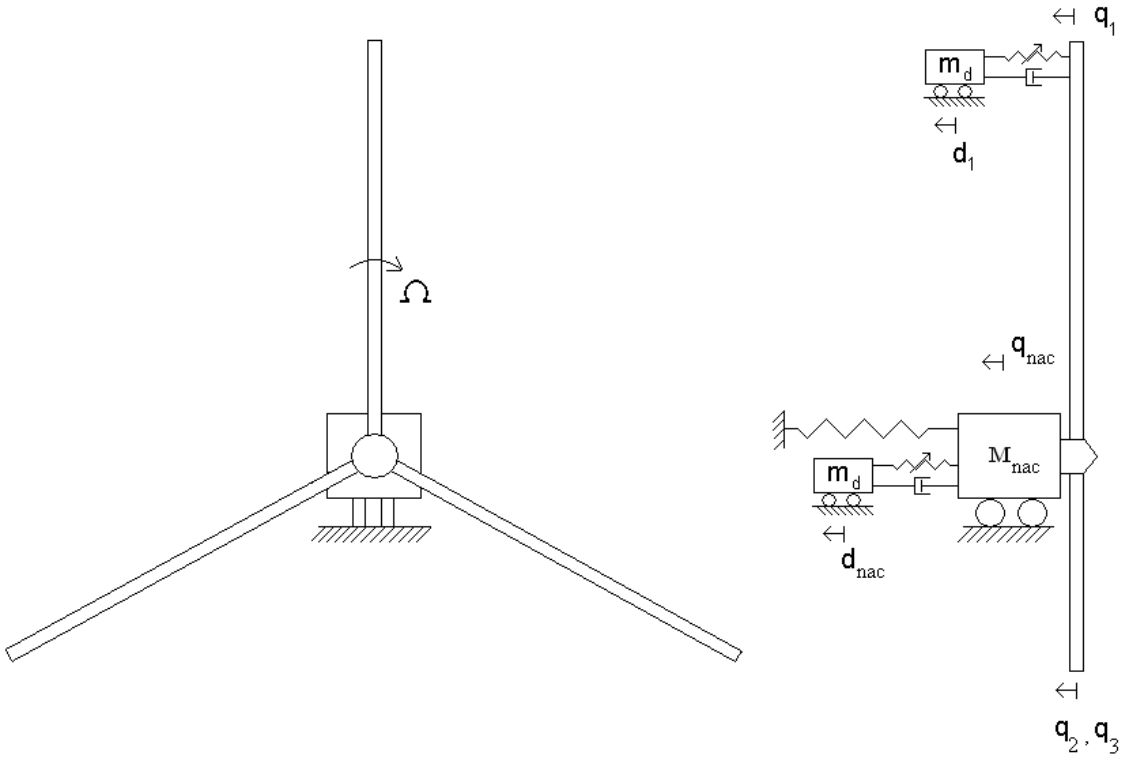

Figure 1

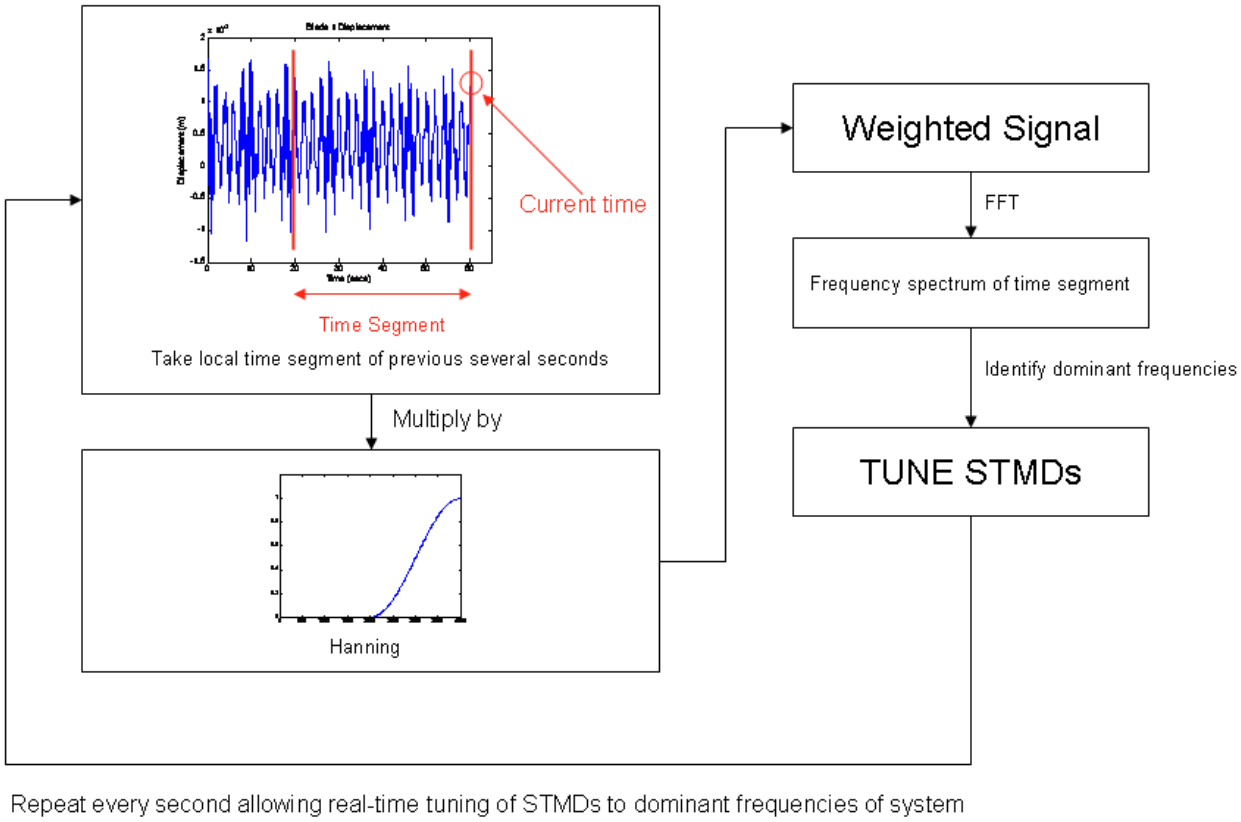

Figure 2

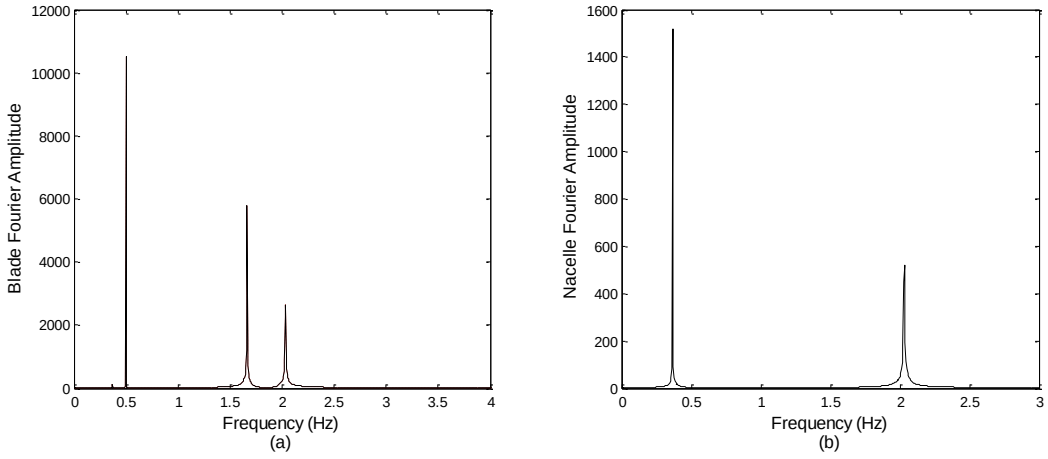

Figure 3

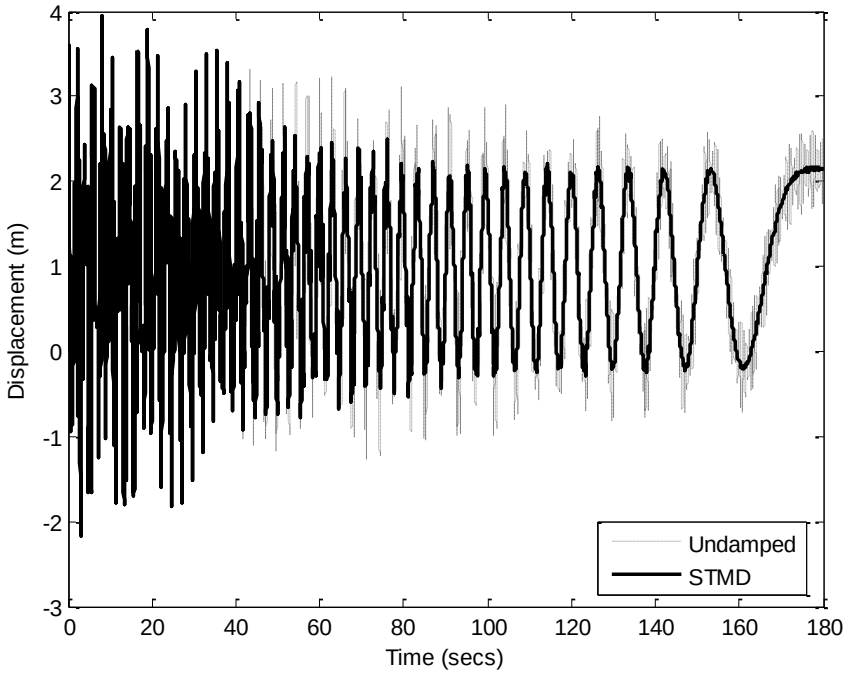

Figure 4a

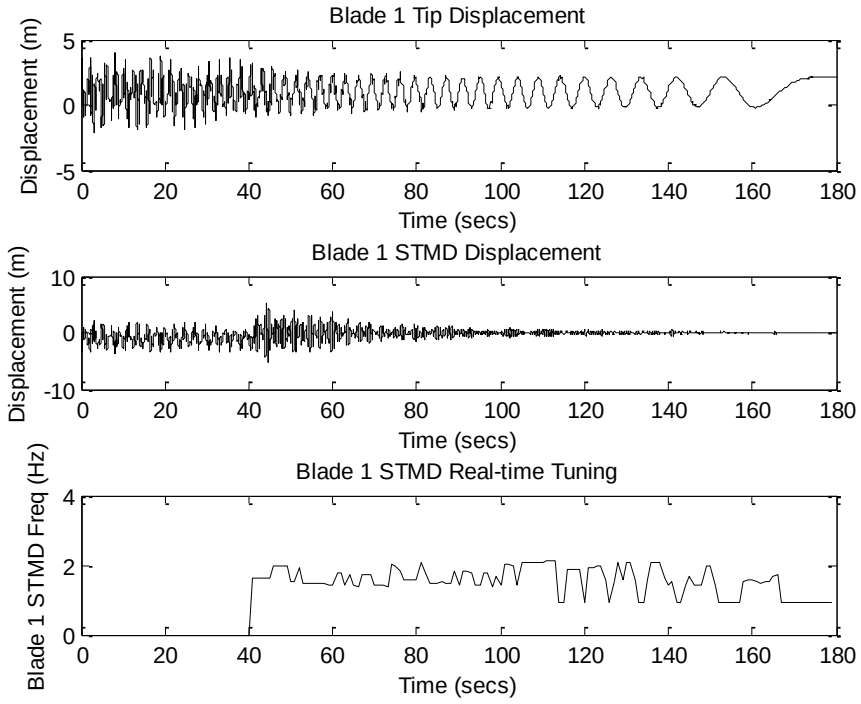

Figure 4b

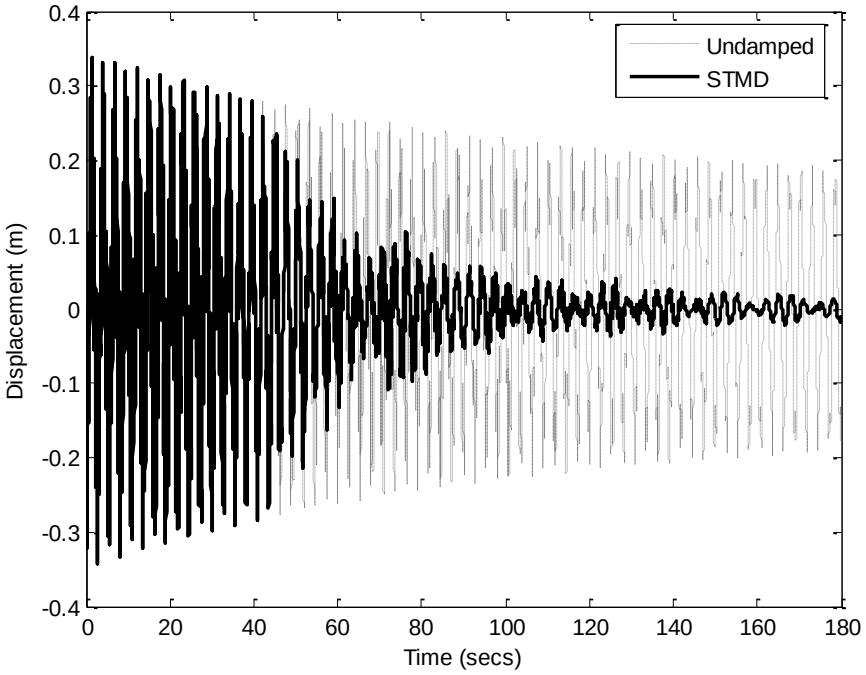

Figure 5a

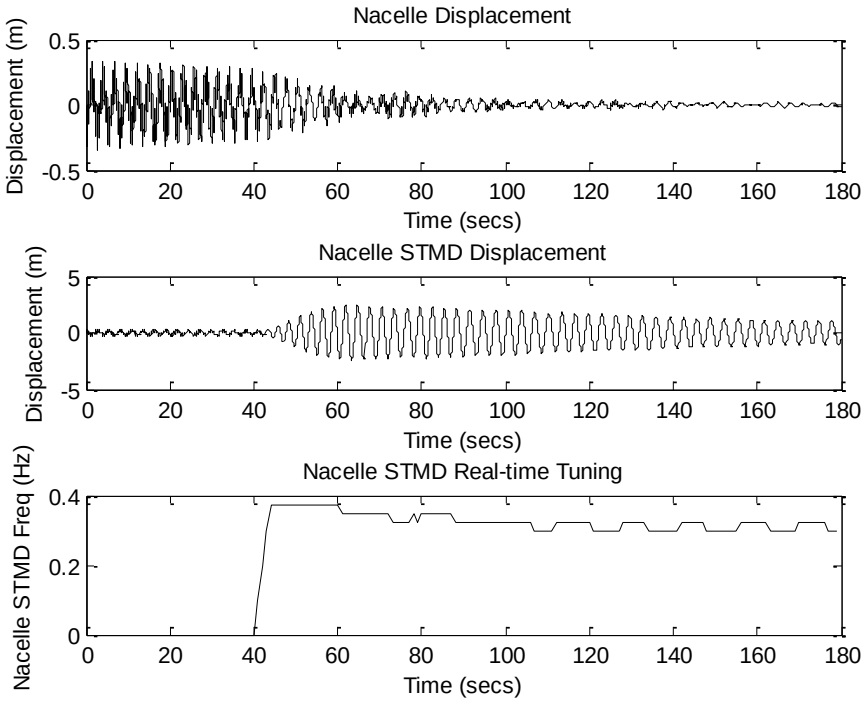

Figure 5b

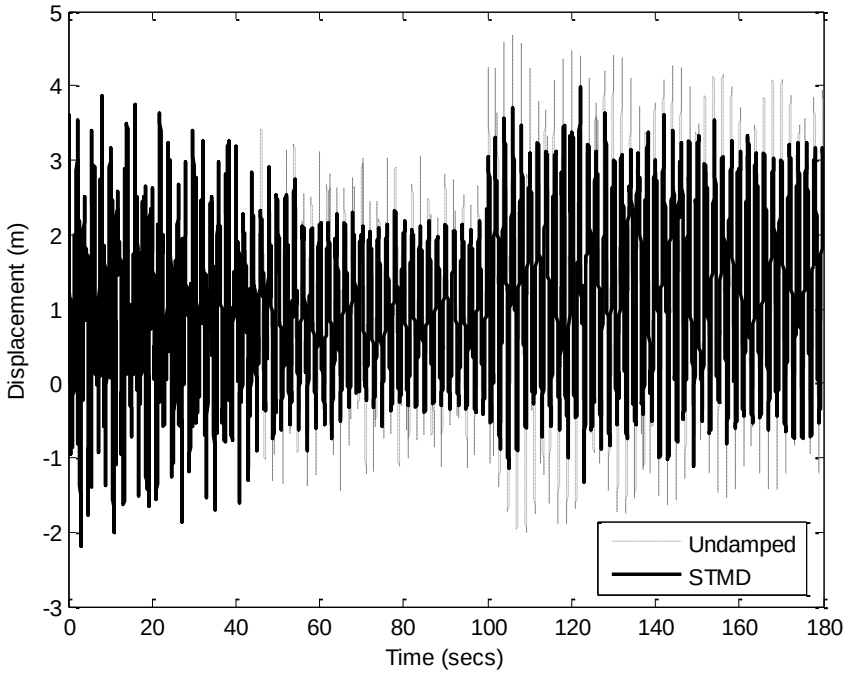

Figure 6a

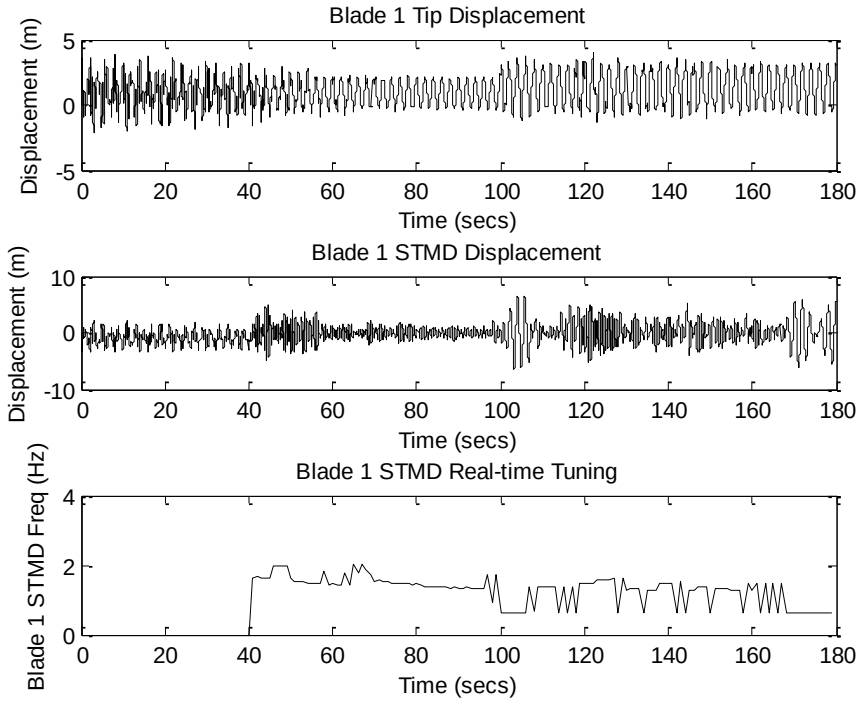

Figure 6b

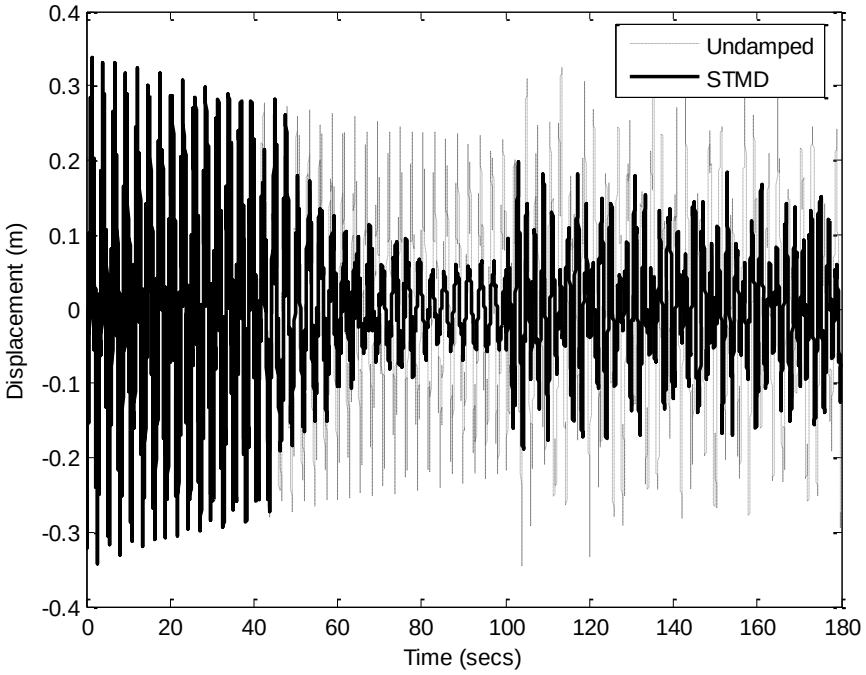

Figure 7a

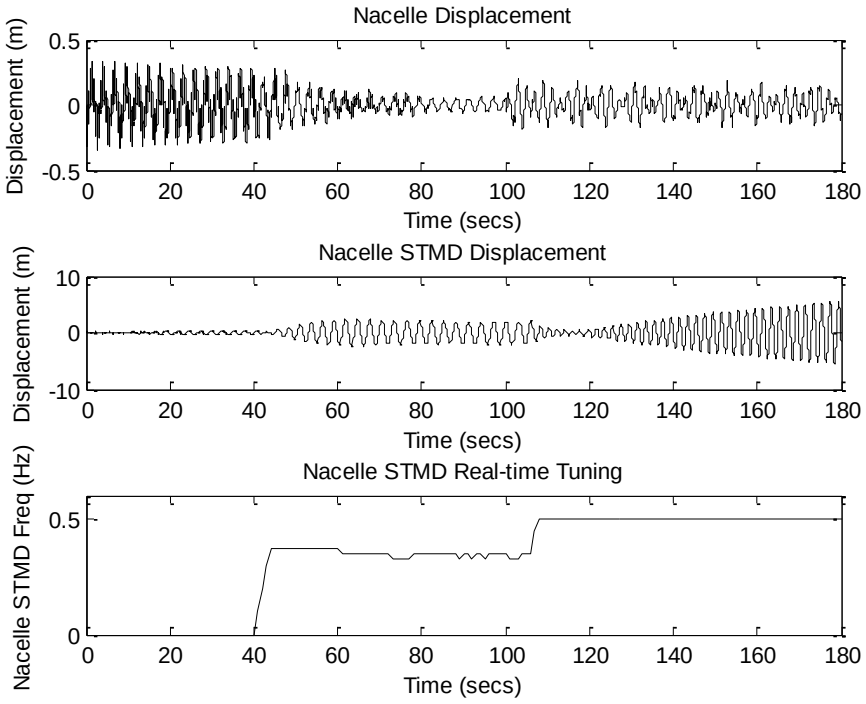

Figure 7b

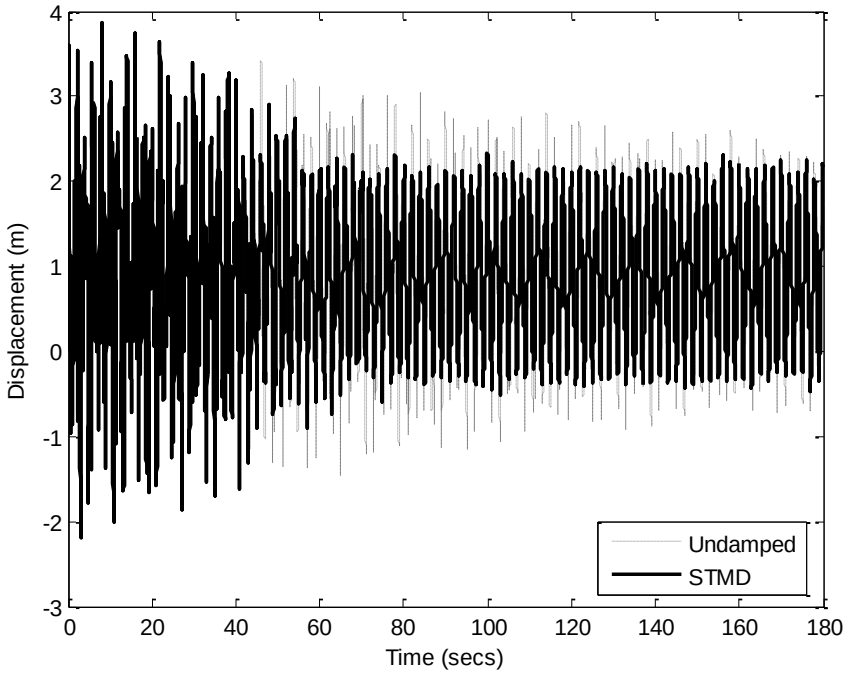

Figure 8a

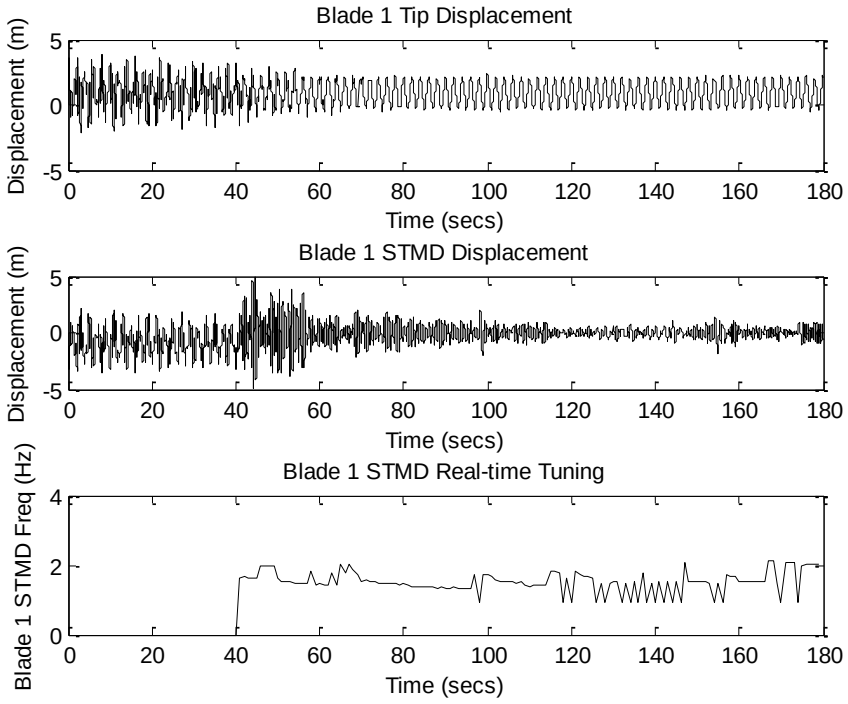

Figure 8b

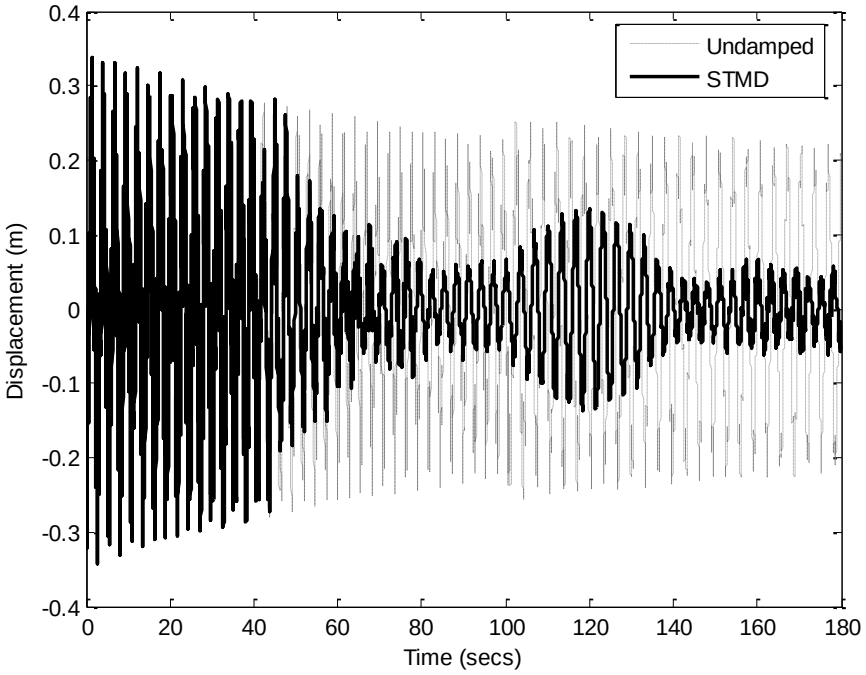

Figure 9a

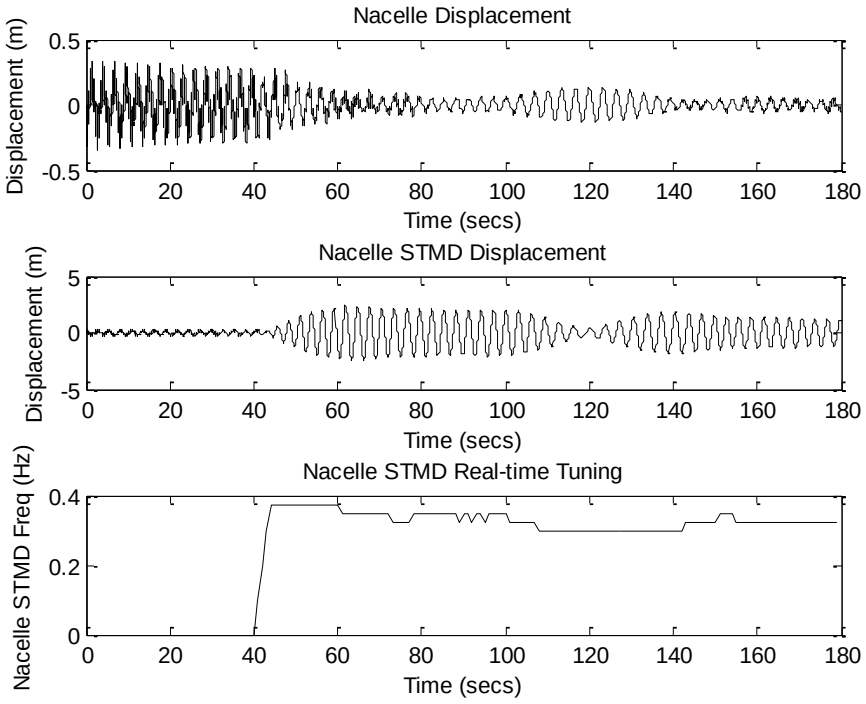

Figure 9b

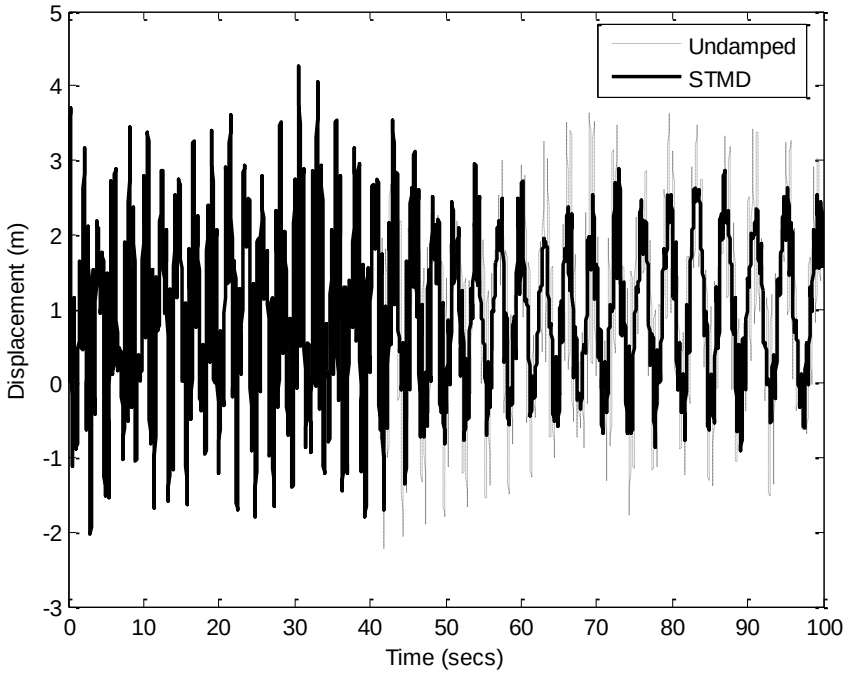

Figure 10a

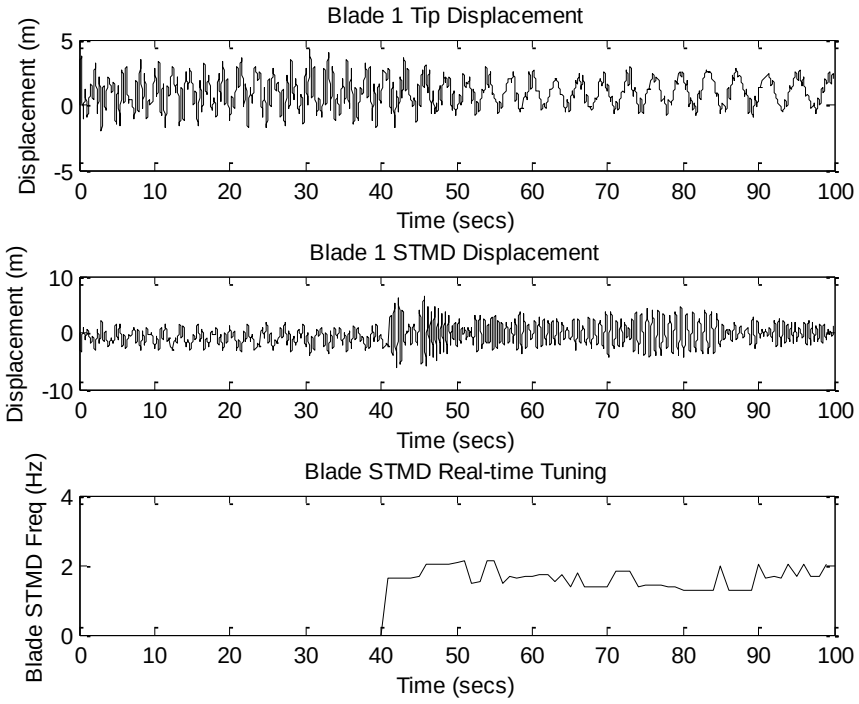

Figure 10b

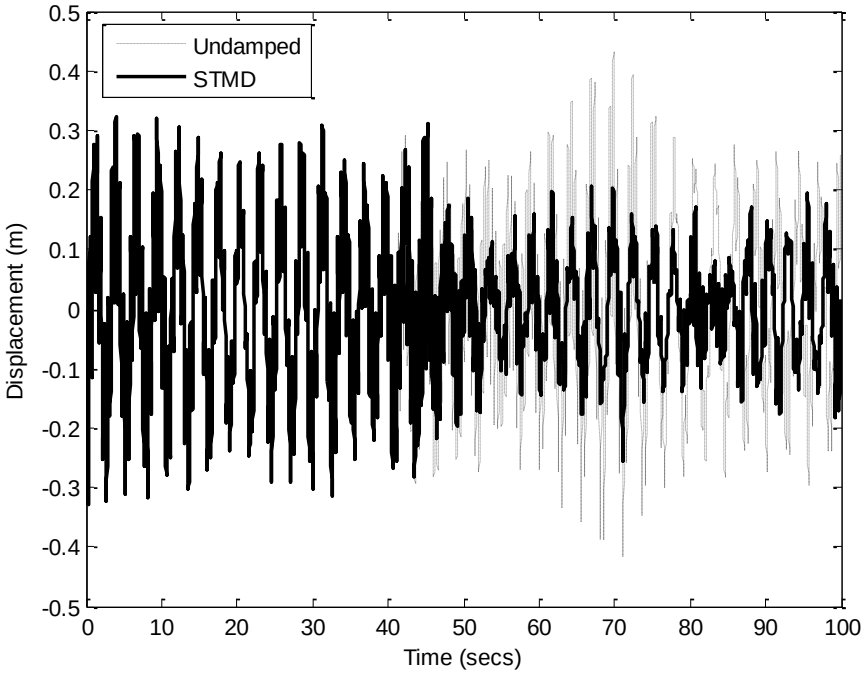

Figure 11a

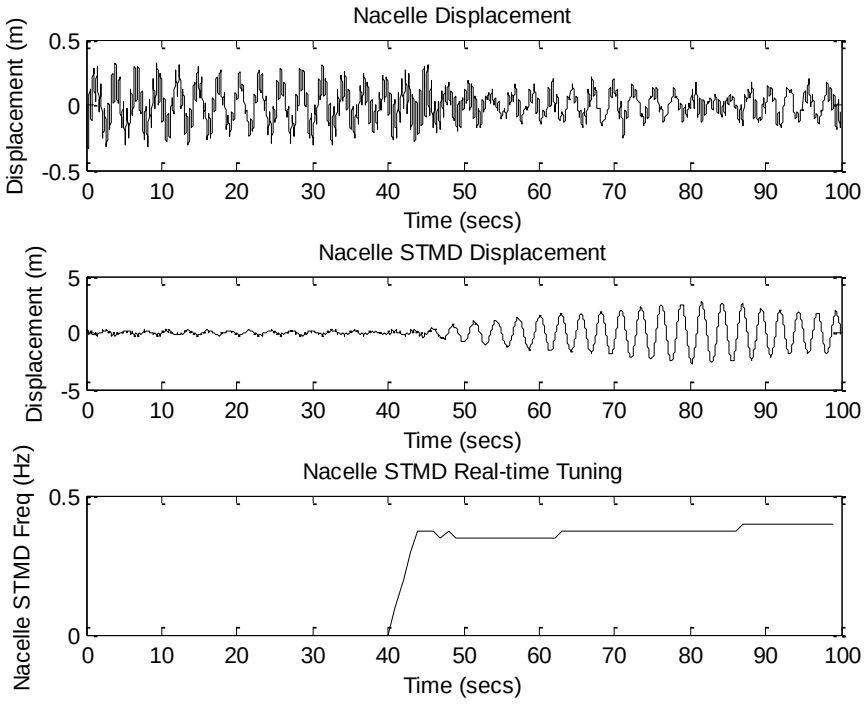

Figure 11b

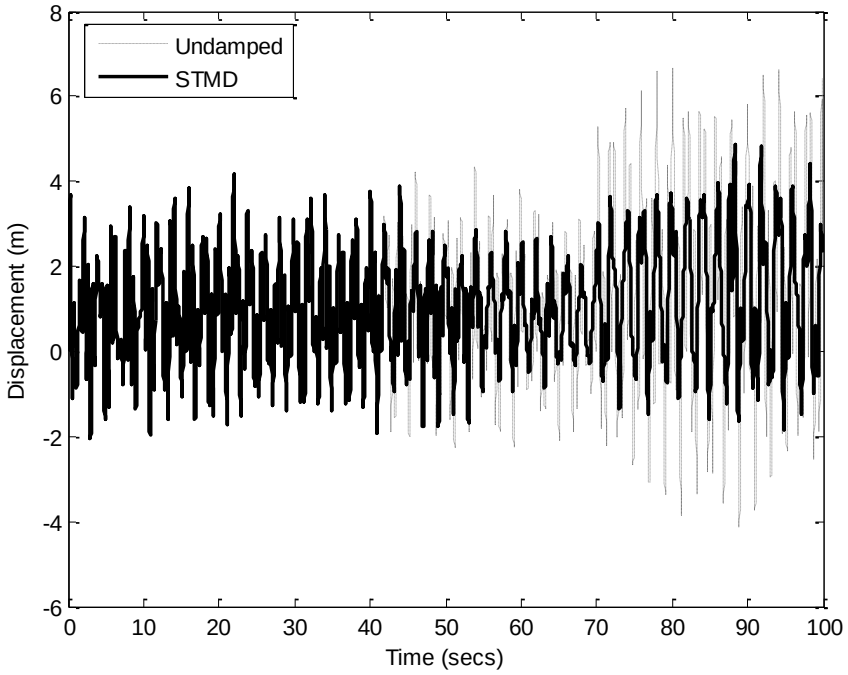

Figure 12a

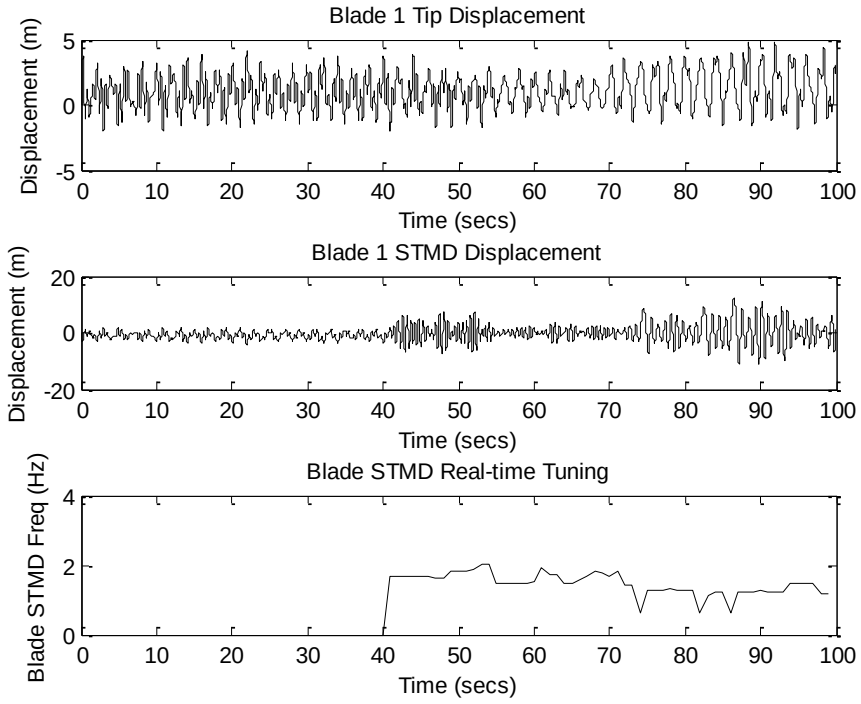

Figure 12b

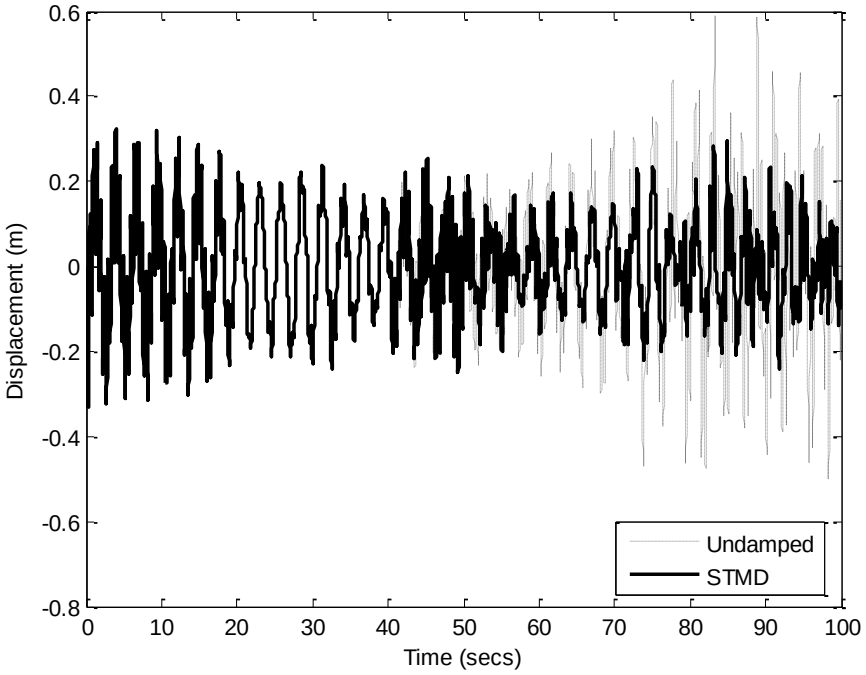

Figure 13a

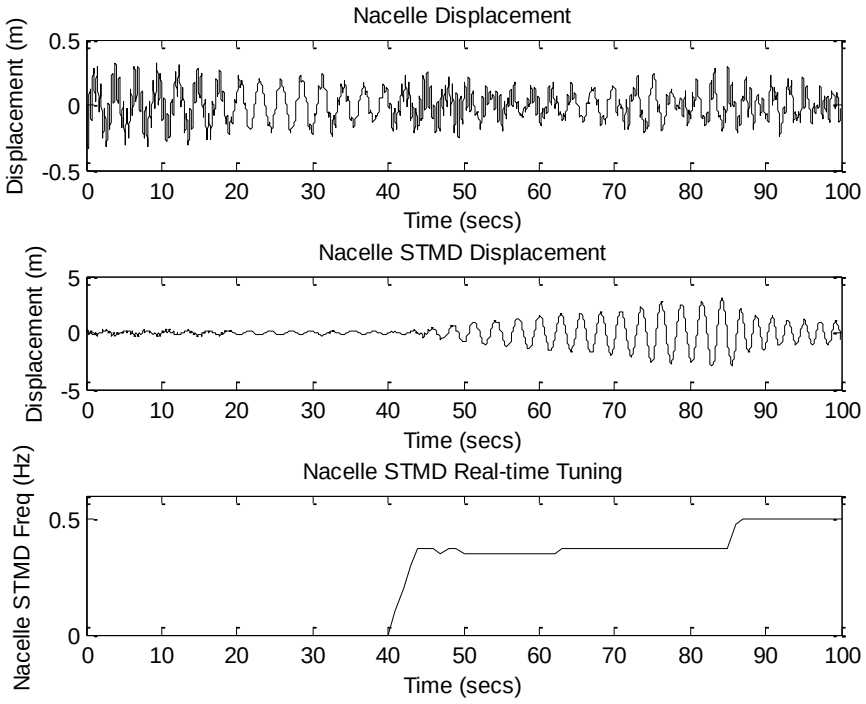

Figure 13b

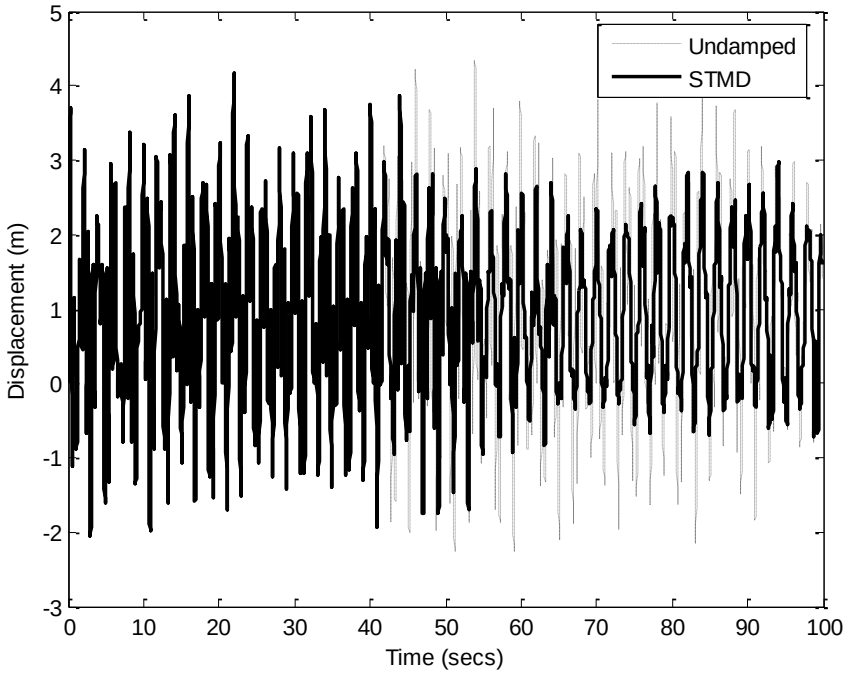

Figure 14a

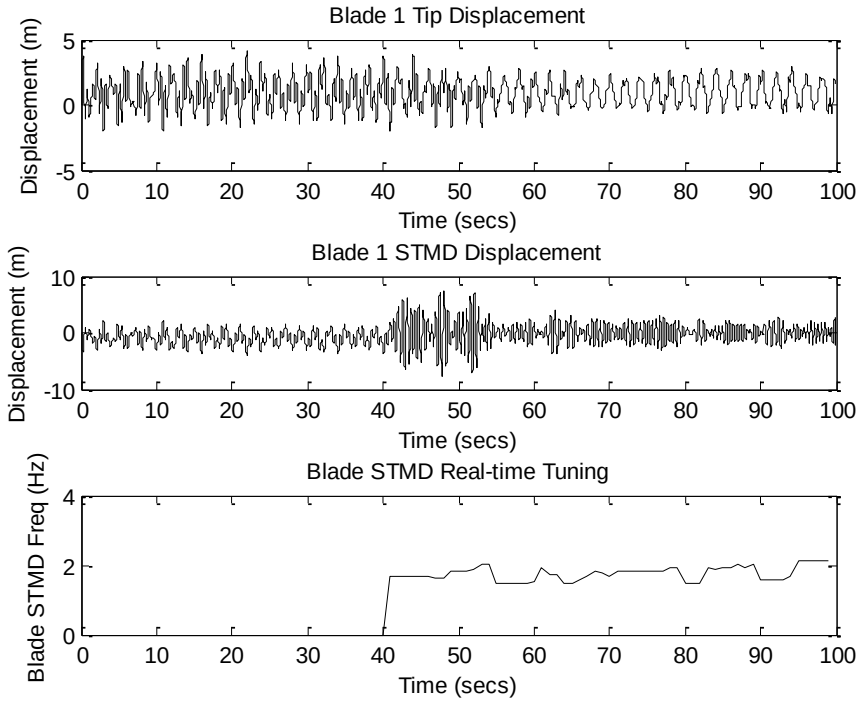

Figure 14b

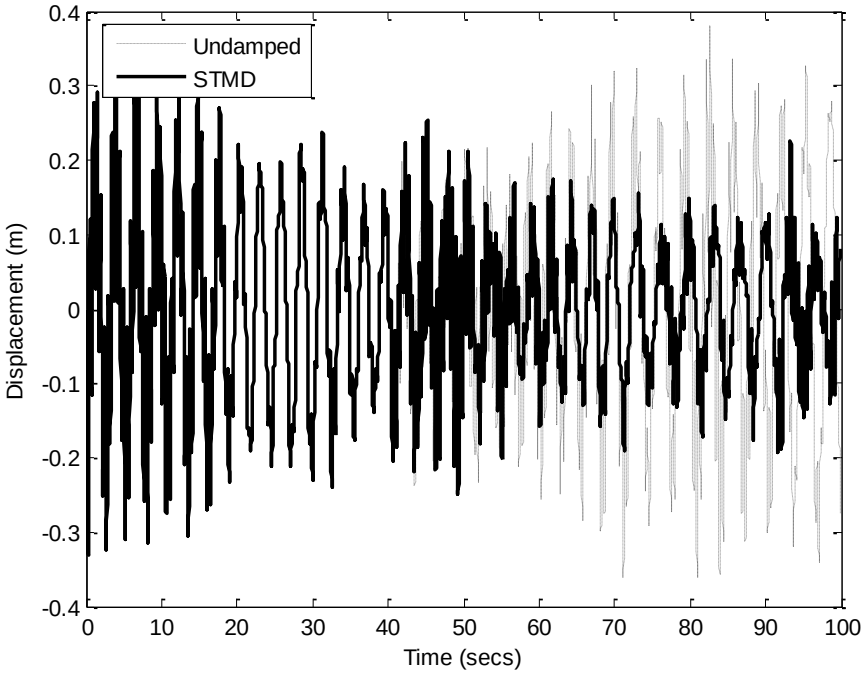

Figure 15a

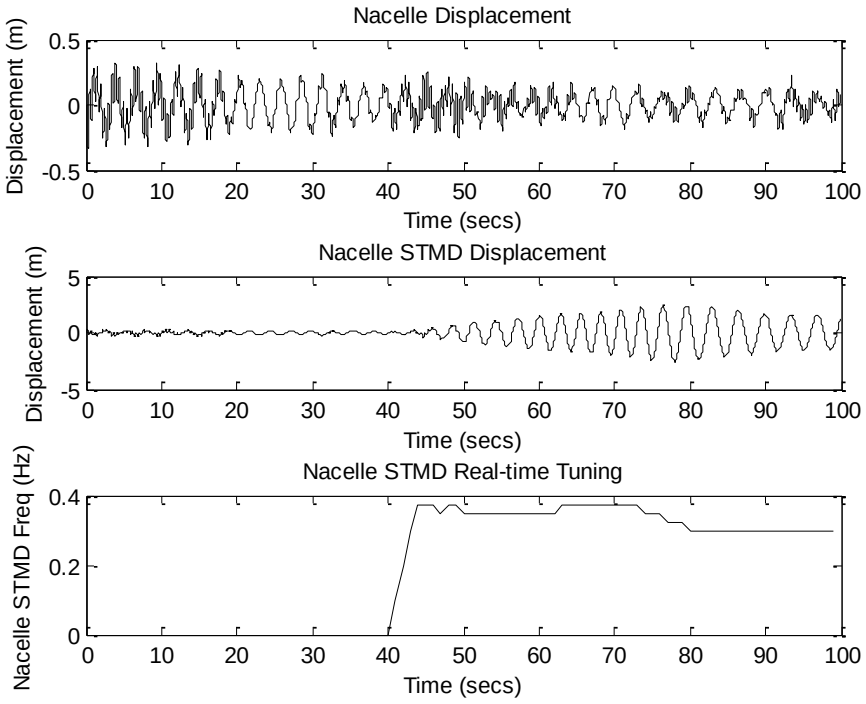

Figure 15b

List of Tables

Table 1 Natural frequency estimates

Ω (Revs/min)	Bernoulli-Euler Frobenius results (Hz)	Lagrangian 1-blade (no coupling) Eigenvalues (Hz)	Lagrangian 3-blades (nacelle coupled) Eigenvalues (Hz)
0	1.5588	1.5588	1.5588, 1.5588, 1.5588
10	1.5703	1.5700	1.5700, 1.5700, 1.9207
60	1.9274	1.9399	1.9394, 1.9394, 2.3649
120	2.8010	2.7863	2.7859, 2.7859, 3.3867

Table 1